in acetonitrile, a Hammett plot showed a linear relationship between Hammett σ_m values and the second reduction potential, indicating that electron density changes on the ligand are transmitted to the metal ions.[10] Replacement of the 4-methyl ring substituent by CF_3 in I and II has been shown to increase $E_{1/2}$ for both one-electron-reduction steps in DMF by 0.14–0.19 V, clearly indicating the transmission of a distant electron-withdrawing effect to the copper centers.[17]

The wide separation of the two reduction waves of all these compounds indicates significant stability for the one-electron intermediates, as is indicated by the large conproportionation constants (Table VII). The one-electron-reduced species derived from I exhibits a seven-line EPR spectrum at room temperature in both CH_2Cl_2 and CH_3CN, indicative of interaction of the odd electron with both copper centers.[6,8] Compound II produces a one-electron-reduced species in CH_3CN, which also exhibits a seven-line spectrum (Figure 6). The analogous copper tetrafluoroborate complex involving the butylene-bridged macrocyclic ligand derived from 4-*tert*-butyl-2,6-diformylphenol has also been shown to produce a one-electron-reduced species in CH_2Cl_2 or acetone, which exhibits a seven-line spectrum at room temperature.[11] This behavior contrasts with that associated with III and IV, which exhibit four-line spectra.[4,30]

Acknowledgment. We thank the Natural Sciences and Engineering Research Council of Canada for financial support for this study, including the purchase of the variable-temperature Faraday susceptometer and EPR spectrometer.

Supplementary Material Available: Tables SI and SII, listing thermal parameters for I and II, Tables SIII and SIV, listing complete bond lengths and angles for I and II, Tables SV and SVI, listing atomic positional parameters for hydrogen atoms in I and II, and Figures S1–S4, illustrating experimental and theoretical susceptibility curves as a function of temperature for II–V (15 pages); tables of calculated and observed structure factors for I and II (50 pages). Ordering information is given on any current masthead page.

(30) Mandal, S. K.; Thompson, L. K.; Nag, K. *Inorg. Chim. Acta* **1988**, *149*, 247.

Contribution from the Anorganisch-Chemisches Institut der Universität, Wilhelm-Klemm-Strasse 8, D-4400 Münster, FRG

Preparation, Structure, and Properties of Manganese Toluene-3,4-dithiolate Complexes in Different Oxidation States

Klaus Greiwe, Bernt Krebs, and Gerald Henkel*

Received August 2, 1988

Anaerobic reaction of $MnCl_2 \cdot 4H_2O$ with toluene-3,4-dithiolate (tdt^{2-}) in methanol yields $[Mn(tdt)_2]^{2-}$, which was isolated as its Ph_4P^+ salt. $[Ph_4P]_2[Mn(tdt)_2] \cdot 2MeOH$ (**1**) crystallizes in the monoclinic space group $P2_1/c$ with $a = 22.378$ (9) Å, $b = 12.102$ (4) Å, $c = 21.888$ (8) Å, $\beta = 110.48$ (3)°, and $Z = 4$. The X-ray structure of **1** was solved by direct methods and refined to R (R_w) = 0.063 (0.060) by using 5755 unique observed reflections ($I \geq 1.96\sigma(I)$). The anion $[Mn(tdt)_2]^{2-}$ features an extremely distorted tetrahedral MnS_4 coordination unit with mean Mn–S bond distances of 2.417 Å and mean S–Mn–S chelate angles of 88.87°. Controlled exposure of methanolic solutions of $[Mn(tdt)_2]^{2-}$ to air results in the immediate formation of a brown-red solution from which black crystals were isolated upon addition of Ph_4PBr. Crystals of $[Ph_4P]_2[Mn(tdt)_2][Mn(tdt)_2MeOH] \cdot 3MeOH$ (**2**) contain homoleptic ($[Mn(tdt)_2]^-$) and heteroleptic ($[Mn(tdt)_2MeOH]^-$) complexes simultaneously. **2** crystallizes in the triclinic space group $P\bar{1}$ with $a = 10.001$ (4) Å, $b = 19.447$ (8) Å, $c = 19.814$ (8) Å, $\alpha = 99.64$ (3)°, $\beta = 90.01$ (3)°, $\gamma = 104.12$ (3)°, and $Z = 2$. The X-ray structure was refined to R (R_w) = 0.041 (0.042) by using 9707 unique observed reflections ($I \geq 1.96\sigma(I)$). The two anions $[Mn(tdt)_2]^-$ and $[Mn(tdt)_2MeOH]^-$ occupy different crystallographic sites. The addition of a methanol molecule to the square-planar MS_4 unit of $[Mn(tdt)_2]^-$ extends the metal coordination to a square pyramid in $[Mn(tdt)_2MeOH]^-$. $[Mn(tdt)_2]^-$ and $[Mn(tdt)_2MeOH]^-$ exhibit mean Mn–S distances of 2.282 and 2.309 Å, respectively. The solid-state magnetic susceptibility of **1** is consistent with a Mn(II) high-spin configuration, while the magnetic data of **2** are indicative of high-spin Mn(III) centers. Spectral properties of solutions prepared from **2** conform to the existence of only one paramagnetic species in solution. The temperature-dependent positions of the isotropically shifted ^1H NMR signals between 220 and 340 K were measured. Assignment of the signals was accomplished by comparison with the analogous benzene-1,2-dithiolate complexes. Room-temperature ^1H NMR spectra for the iron/tdt^{2-} complexes are provided and compared with the spectra of the manganese compounds. Cyclic voltammetry and polarography in different solvents confirm the one-electron transfer for the Mn(II)/Mn(III) redox couple. The ΔE_p values are strongly affected by the nature of the electrode. A Pt electrode provides much larger peak separations in the CV spectra than a glassy-carbon electrode. Stronger coordinating solvents induce cathodically shifted $E_{1/2}$ potentials.

Introduction

In the last three decades there has been a great increase of knowledge in the chemistry of transition-metal–sulfur complexes. The coordination chemistry of several different classes of sulfur-containing ligands was investigated. Most interest was first attracted by 1,1-dithio[1] and 1,2-dithiolene[2] ligands. Especially, the assignment of oxidation states to the metal centers in the redox-active dithiolene type complexes has been and still is[3] a point of great interest. Later, the transition-metal–sulfur chemistry was largely influenced by bioinorganic aspects. To synthesize model compounds for active centers in nonheme iron–sulfur proteins and to mimic the ligation properties of cysteinyl residues in proteins were the most stimulating impetuses for the rapidly evolving thiolate (RS^-) chemistry.[4] Due to this biochemical background[5] most work was first done on iron–sulfide–thiolate clusters and iron–thiolate complexes[6] followed by the rapid exploration of the

(1) Coucouvanis, D. *Prog. Inorg. Chem.* **1970**, *11*, 233; **1979**, *26*, 301.
(2) (a) Typical 1,2-dithiolene ligands include benzene-1,2-dithiolate (bdt^{2-}), toluene-3,4-dithiolate (tdt^{2-}), tetrachlorobenzene-1,2-dithiolate ($S_2C_6Cl_4^{2-}$), 1,2-dimethylbenzene-4,5-dithiolate (xdt^{2-}), *cis*-ethylene-1,2-dithiolate ($endt^{2-}$), maleonitriledithiolate (mnt^{2-}), and bis(methoxycarbonyl)ethene-1,2-dithiolate. (b) McCleverty, J. A. *Prog. Inorg. Chem.* **1968**, *10*, 49. (c) Schrauzer, G. N. *Acc. Chem. Res.* **1969**, *2*, 72. (d) Eisenberg, R. *Prog. Inorg. Chem.* **1970**, *12*, 295. (e) Hoyer, E.; Dietzsch, W.; Schroth, W. *Z. Chem.* **1971**, *11*, 41. (f) Burns, R. P.; McAuliffe, C. A. *Adv. Inorg. Chem. Radiochem.* **1979**, *22*, 303. (g) Ibers, J. A.; Pace, L. J.; Martinsen, J.; Hoffman, B. M. *Struct. Bonding (Berlin)* **1982**, *50*, 1.
(3) Sawyer, D. T.; Srivatsa, G. S.; Bodini, M. E.; Schaefer, W. P.; Wing, R. M. *J. Am. Chem. Soc.* **1986**, *108*, 936.
(4) Dance, I. G. *Polyhedron* **1986**, *5*, 1037.
(5) (a) Beinert, H.; Thompson, A. J. *Arch. Biochem. Biophys.* **1983**, *222*, 333. (b) Lovenberg, W., Ed. *Iron-Sulfur Proteins*; Academic Press: New York, 1973, 1977; Vols. I–III. (c) Spiro, T. G., Ed. *Iron-Sulfur Proteins*; Wiley: New York, 1982.

0020-1669/89/1328-3713$01.50/0

thiolate coordination chemistry of other transition and main-group elements.[4]

The manganese thiolato complexes $[Mn(SPh)_4]^{2-}$,[7,8] $[MnCl(SPh)_3]^{2-}$,[9] $[Mn(edt)_2]^{2-}$,[8] $[Mn_4(SPh)_{10}]^{2-}$,[8] $[Mn_2(S\text{-}o\text{-}xyl)_2X_2]^{2-}$ (X = PhS^-, $Et_2NCS_2^-$; X_2 = S_2-*o*-xyl^{2-}),[9] and $[Mn_2(edt)_4]^{2-}$[8,10] are well characterized. However, the field of homoleptic manganese dithiolene complexes is comparably undeveloped. For Mn(IV) only two mononuclear complexes, namely $[Mn(mnt)_3]^{2-}$[2,11] and $[Mn(S_2C_6Cl_4)_3]^{2-}$,[2,12] have been reported. For Mn(III) some pyridine adducts with the dithiolene type ligands xdt^{2-} and $endt^{2-}$ were prepared.[13] Especially, the manganese complexes with tdt^{2-} ligands were not completely characterized[12] or their composition was not exactly defined.[14] The present investigation was therefore initiated to uncover the unexplored coordination chemistry of tdt^{2-} with manganese in different oxidation states. In view of the well-developed thiolate chemistry of the first-row transition metals with ethane-1,2-dithiolate ligands (edt^{2-})[8,10,15-17] and the electronical ambiguity of the dithiolene ligand tdt^{2-}, we extended our study to other elements. This paper contributes therefore to the discussion of formal oxidation states in metal/tdt^{2-} complexes in comparison to metal/edt^{2-} complexes. Recently, we have briefly described our initial results[18] on the manganese/tdt^{2-} system. Reported here are the syntheses, structures, and several other properties of Mn(II,III)/tdt^{2-} and Fe(II,III)/tdt^{2-} complexes.

Experimental Section

Synthesis. All operations were carried out under a pure dinitrogen atmosphere in a glovebox. The extremely air-sensitive M(II)/tdt^{2-} complexes (M = Fe, Mn) were prepared by conventional Schlenk techniques. Solvents were dried over and distilled from appropriate drying agents. Benzene-1,2-dithiol was prepared by a literature method.[19] Other chemicals were used as purchased.

$[Ph_4P]_2[Mn(tdt)_2]\cdot 2MeOH$ (1). To a solution of 0.99 g (5 mmol) of $MnCl_2\cdot 4H_2O$ in 75 mL of methanol was added dropwise a solution of 0.46 g (20 mmol) of sodium and 1.56 g (10 mmol) of toluene-3,4-dithiol in 75 mL of methanol, causing a yellow color. The reaction mixture was filtered and treated with 4.20 g (10 mmol) of Ph_4PBr. Large yellow, block-shaped crystals separated, which were suitable for X-ray analysis. The product was washed with 50 mL of degassed cold water, twice with 25 mL of methanol, and then with ether. Yield: 3.75 g (68%).

Anal. Calcd for $C_{64}H_{60}O_2P_2S_4Mn$: C, 69.48; H, 5.47; Mn, 11.59. Found: C, 69.31; H, 5.48; Mn, 11.94.

$[Ph_4P]_2[Mn(tdt)_2][Mn(tdt)_2MeOH]\cdot 3MeOH$ (2). To a solution of 0.99 g (5 mmol) of $MnCl_2\cdot 4H_2O$ in 75 mL of methanol was added a solution of 0.46 g (20 mmol) of sodium and 1.56 g (10 mmol) of toluene-3,4-dithiol in 75 mL of methanol. The stirred solution was then exposed to air for 2 min, causing an immediate change to brown-red. The solution was stirred for 2 h at room temperature under nitrogen and then stored for 3 days at −30 °C. The brown solid was filtered off, and 2.10 g (10 mmol) of solid Ph_4PBr was added to the clear brown-red filtrate. The black plate-shaped crystals, which separated overnight, were filtered off and washed with 50 mL of degassed water and 50 mL of methanol. These crystals were suitable for X-ray analysis. Yield: 2.91 g (76%).

Anal. Calcd for $C_{80}H_{80}O_4P_2S_8Mn_2$: C, 62.65; H, 5.26; Mn, 7.16. Found: C, 62.91; H, 5.19; Mn, 7.74.

$[Ph_4P][Mn(bdt)_2]$. Preparation was as described for **2**; instead of toluene-3,4-dithiol 1.42 g (10 mmol) of benzene-1,2-dithiol ($bdtH_2$) was used. Yield: 2.02 g (60%).

Anal. Calcd for $C_{36}H_{28}PS_4Mn$: C, 64.08; H, 4.18. Found: C, 64.01; H, 4.26.

$[Ph_4P]_2[Fe_2(tdt)_4]$. To a solution of 0.81 g (5 mmol) of $FeCl_3$ in 50 mL of methanol was added slowly a solution of 10 mmol of $Na_2S_2C_6H_3Me$ (from 0.46 g (20 mmol) of sodium and 1.56 g (10 mmol) of toluene-3,4-dithiol) in 80 mL of methanol. The deep red solution was treated with 2.10 g (10 mmol) of solid Ph_4PBr. The black crystalline solid was collected and washed thoroughly with water and subsequently with methanol and ether. Yield: 2.40 g (68%).

Anal. Calcd for $C_{76}H_{64}P_2S_8Fe_2$: C, 64.86; H, 4.58. Found: C, 64.95; H, 4.71.

$[Ph_4P]_2[Fe(tdt)_2]$. A 10-mmol amount of $Na_2S_2C_6H_3Me$ (from 0.46 g (20 mmol) of sodium and 1.56 g (10 mmol) of toluene-3,4-dithiol) in 75 mL of methanol was added slowly to a suspension of 0.63 g (10 mmol) of anhydrous $FeCl_2$ in 75 mL of methanol. A 4.20-g amount (10 mmol) of solid Ph_4PBr was added to the brown filtrate of the reaction mixture. Standing overnight afforded 2.91 g (55%) of a deep brown microcrystalline solid, which was washed with degassed water and methanol.

Anal. Calcd for $C_{62}H_{52}P_2S_4Fe$: C, 71.39; H, 5.02. Found: C, 71.05; H, 5.06.

Collection and Reduction of X-ray Data. Crystals of $[Ph_4P]_2[Mn(tdt)_2]\cdot 2MeOH$ (**1**) and $[Ph_4P]_2[Mn(tdt)_2][Mn(tdt)_2MeOH]\cdot 3MeOH$ (**2**) suitable for X-ray diffraction were obtained from the filtered reaction solutions by addition of solid Ph_4PBr. The crystals were fixed with a trace of silicone grease at the top of glass capillaries and cooled by a stream of nitrogen with use of a modified Syntex LT-1 low-temperature device (143 K). All data were collected on a Syntex $P2_1$ four-circle automated diffractometer equipped with a graphite monochromator, a Mo Kα source, and a scintillation counter. The $\theta/2\theta$-scan mode was used for all data collections. The unit cell parameters with standard deviations were derived from a least-squares fit of the scattering angles of 15 centered reflections in the range $20° \le 2\theta \le 30°$. The intensity of one standard reflection measured every 99 scans did not show any significant changes during data collection for **2**. Due to a short interruption of the cold nitrogen stream during data collection for **1**, a reduction of the

Table I. Crystallographic Data for $[Ph_4P]_2[Mn(tdt)_2]\cdot 2MeOH$ (**1**) and $[Ph_4P]_2[Mn(tdt)_2][Mn(tdt)_2MeOH]\cdot 3MeOH$ (**2**)

compd	**1**	**2**
chem formula	$C_{64}H_{60}O_2P_2S_4Mn$	$C_{80}H_{80}O_4P_2S_8Mn_2$
fw	1106.34	1533.87
a, Å	22.378 (9)	10.001 (4)
b, Å	12.102 (4)	19.447 (8)
c, Å	21.888 (8)	19.814 (8)
α, deg		99.64 (3)
β, deg	110.48 (3)	90.01 (3)
γ, deg		104.12 (3)
V, Å^3	5553	3681
Z	4	2
space group	$P2_1/c$ (No. 14)	$P\bar{1}$ (No. 2)
T, K	143	143
λ, Å	0.710 69	0.710 69
ρ_{calcd}, g cm^{-3}	1.323	1.384
ρ_{obs}, g cm^{-3} (293 K)	1.29	1.34
μ, cm^{-1}	5.0	6.7
$R(F)$	0.063	0.041
$R_w(F)$	0.060	0.042

(6) (a) Strasdeit, H.; Krebs, B.; Henkel, G. *Inorg. Chem.* **1984**, *23*, 1816. (b) Snyder, B. S.; Holm, R. H. *Inorg. Chem.* **1988**, *27*, 2339 and literature cited therein. (c) Kanatzidis, M. G.; Salifoglou, A.; Coucouvanis, D. *Inorg. Chem.* **1986**, *25*, 2460 and literature cited therein. (d) Hagen, K. S.; Holm, R. H. *Inorg. Chem.* **1984**, *23*, 418. (e) Henkel, G.; Tremel, W.; Krebs, B. *Angew. Chem.* **1983**, *95*, 317; *Angew. Chem., Int. Ed. Engl.* **1983**, *22*, 319; *Angew. Chem., Suppl.* **1983**, 323. (f) Henkel, G.; Tremel, W.; Krebs, B. *Angew. Chem.* **1981**, *93*, 1072; *Angew. Chem., Int. Ed. Engl.* **1981**, *20*, 1033.

(7) Swenson, D.; Baenziger, N. C.; Coucouvanis, D. *J. Am. Chem. Soc.* **1978**, *100*, 1932.

(8) Costa, T.; Dorfman, J. R.; Hagen, K. S.; Holm, R. H. *Inorg. Chem.* **1983**, *22*, 4091.

(9) Greiwe, K.; Krebs, B.; Henkel, G. Unpublished results. S_2-*o*-xyl^{2-} = *o*-xylene-α,α'-dithiolate.

(10) Christou, G.; Huffman, J. C. *J. Chem. Soc., Chem. Commun.* **1983**, 558.

(11) (a) McCleverty, J. A.; Locke, J.; Wharton, E. J.; Gerloch, M. *J. Chem. Soc., Dalton Trans.* **1968**, 816. (b) Stiefel, E. I.; Bennet, L. E.; Dori, Z.; Crawford, T. H.; Simo, C.; Gray, H. B. *Inorg. Chem.* **1970**, *2*, 281.

(12) Wharton, E. J.; McCleverty, J. A. *J. Chem. Soc., Dalton Trans.* **1969**, 2258.

(13) Hoyer, E.; Dietzsch, W.; Müller, H. *Z. Chem.* **1967**, *7*, 354.

(14) Kaneko, M.; Ishihara, N.; Yamada, A. *Makromol. Chem.* **1981**, *182*, 89.

(15) Pulla Rao, Ch.; Dorfman, J. R.; Holm, R. H. *Inorg. Chem.* **1986**, *25*, 428.

(16) (a) Szeymies, D.; Krebs, B.; Henkel, G. *Angew. Chem.* **1983**, *95*, 903; *Angew. Chem., Int. Ed. Engl.* **1983**, *22*, 885; *Angew. Chem., Suppl.* **1983**, 1176. (b) Wiggins, R. W.; Huffman, J. C.; Christou, G. *J. Chem. Soc., Chem. Commun.* **1983**, 1313. (c) Dorfman, J. R.; Holm, R. H. *Inorg. Chem.* **1983**, *22*, 3179.

(17) (a) Snow, M. R.; Ibers, J. A. *Inorg. Chem.* **1973**, *12*, 249. (b) Herskovitz, T.; DePamphilis, B. V.; Gillum, W. O.; Holm, R. H. *Inorg. Chem.* **1975**, *14*, 1426.

(18) Henkel, G.; Greiwe, K.; Krebs, B. *Angew. Chem.* **1985**, *97*, 113; *Angew. Chem., Int. Ed. Engl.* **1985**, *24*, 117.

(19) Degani, I.; Fochi, R. *Synthesis* **1976**, 471.

(20) Weiss, A.; Witte, A. *Magnetochemie*; Verlag Chemie: Weinheim, West Germany, 1973.

(21) Earnshaw, A. *Introduction of Magnetochemistry*; Academic Press: London, New York, 1968.

scattering power by 12% was observed after recentering, which has been accounted for by an appropriate scaling factor for the affected 2680 reflections. An empirical absorption correction (ψ-scan) was applied to the data set of **1**; the data set of **2** was left uncorrected due to minor variations of the ψ-scan intensities. The raw intensity data were corrected for Lorentz and polarization effects according to $F_o^2 = I/Lp$. I is defined as $[S - (t_S/2t_B)(B_1 + B_2)]s$, where S, B_1, and B_2 are the scan and individual background counts, respectively, t_S and t_B are their counting times, and s is the scan speed for the reflection. The variance of I was calculated as $\sigma(I)^2 = [S + (t_S/2t_B)^2(B_1 + B_2)]s$. Further details relevant to the data collections and structure refinements are collected in Table I.

Structure Solution and Refinement. All calculations were performed on a Data General ECLIPSE S/200 minicomputer using the XTL and SHELXTL program packages.[22a,b] Atomic scattering factors for spherical neutral free atoms (bonded for hydrogen) were taken from standard sources.[22c] Both the f' and f'' components of the anomalous dispersion[22c] were included for all non-hydrogen atoms. The function minimized during refinements was $\sum w(|F_o| - |F_c|)^2$, w being defined as $w = [\sigma^2(F_o) + (0.01F_o)^2]^{-1}$ with $\sigma(F_o) = \sigma(I)/(2|F_o|Lp)$. The final R values are given in Table I. They are defined as $R = \sum||F_o| - |F_c||/\sum|F_o|$ and $R_w = [\sum w(|F_o| - |F_c|)^2/\sum w|F_o|^2]^{1/2}$. Individual structure solutions and refinements are briefly described in the following.

$[Ph_4P]_2[Mn(tdt)_2]\cdot 2MeOH$. The structure was solved by direct methods (MULTAN[23]), which revealed the positions of the metal, sulfur, and phosphorus atoms. The remaining non-hydrogen atoms were located from difference Fourier maps computed after least-squares refinement cycles. The positions of the aromatic hydrogen atoms were calculated (d(C–H) = 0.96 Å). The hydrogen atoms of the methyl groups were located from a difference Fourier map upon convergence of the anisotropic refinement of all non-hydrogen atoms. All these hydrogen atoms were then included in the structure factor calculations in fixed positions with $B = 3.5$ Å^2. The asymmetric unit contains two cations, one anion, and two methanol molecules, all of which behaved well during refinements. It was realized later that **1** is isostructural with $[Ph_4P]_2[Cd(tdt)_2]\cdot 2EtOH$[24] and $[Ph_4P]_2[Hg(tdt)_2]\cdot 2MeOH$.[25] Final R factors and other details are included in Table I. Positional parameters of the $[Mn(tdt)_2]^{2-}$ anion are listed in Table II, and selected interatomic distances and angles are compiled in Table III. Atomic parameters of the $[Mn(tdt)_2]^{2-}$ anion, the Ph_4P^+ cations, and solvate molecules, a complete list of distances and angles, and observed and calculated structure factors are provided in Tables S-I, S-II, and S-III, respectively (supplementary material).

$[Ph_4P]_2[Mn(tdt)_2][Mn(tdt)_2MeOH]\cdot 3MeOH$. The distribution of E values is characterized by very strong reflections in the parity groups eee and ooo (mean $\bar{E}^2$: 2.49), moderately strong ones in the parity groups eeo and ooe (mean $\bar{E}^2$: 1.12), and very weak reflections in the remaining parity groups eoo, eoe, oee, and oeo (mean $\bar{E}^2$: 0.19) indicating the presence of a superstructure with a C-centered subcell, which is itself the pseudosupercell of an F-centered subsubcell. The principal features of the heavy-atom distribution were obtained by direct methods (MULTAN[23]), neglecting all superstructure reflections (space group $F\bar{1}$). The (averaged) model revealed in this way was a MnS_6 octahedron located on a center of symmetry. The MnS_6 octahedron is the result of the superposition of two planar MnS_4 units that are perpendicular to each other and share a common S–Mn–S diagonal. Changing the space group to $C\bar{1}$ resulted in two crystallographically independent planar MnS_4 units both occupying centers of symmetry. At this stage the carbon atoms of the tdt^{2-} ligands as well as all non-hydrogen atoms of the cation, a methanol molecule bonded to one of the Mn sites (statistically disordered), and another (noncoordinated) methanol molecule could successfully be resolved from a difference Fourier map. Isotropic refinement of this structural model converged to $R = 0.1$. In the final stage of the structure solution process the model was transformed with respect to the symmetry requirements of the space group $P\bar{1}$, resulting in the loss of inversion centers associated with the manganese positions. Successive refinement cycles followed by difference Fourier syntheses revealed the positions of the non-hydrogen atoms of an additional noncoordinated methanol molecule as well as the positions of the hydrogen atoms of the anions, the cations, the coordinated methanol molecules, and half of the remaining noncoordinated methanol molecules. They were added to the structure model. In the final refinement cycles the coordinates of these atoms were refined together with individual temperature factors (isotropic for the H atoms, otherwise anisotropic). The coordinates of the H atom of the bonded hydroxo group were fixed. Final R factors and other details are included in Table I. Atomic coordinates of the $[Mn(tdt)_2]^-$ and $[Mn(tdt)_2MeOH]^-$ anions are compiled in Table IV, and selected interatomic distances and angles of the anions are listed in Table V. Atomic parameters of the anions, cations, and solvate molecules, a complete list of distances and angles, and observed and calculated structure factors are provided in Tables S-IV, S-V, and S-VI, respectively (supplementary material).

Other Physical Measurements. All samples were prepared and measured under anaerobic conditions. Cyclic voltammetric experiments were first carried out with Pt-flag electrodes (working and auxiliary electrode), a Bank Elektronik Potentioscan Wenking POS73 potentiostat, and a Kipp & Zonen x-y recorder BD90. Polarographic measurements were performed with a Metrohm E505/E506 polarograph. These measurements provided the results reported in ref 18. In subsequent investigations voltammetric and polarographic measurements were reconducted with a Metrohm VA-Scanner, a Metrohm 626 Polarecord, and a Metrohm 663 VA-Stand equipped with a glassy-carbon auxiliary electrode, using a glassy-carbon and a Pt-working electrode, respectively. All potentials reported in this paper are obtained at room temperature relative to a saturated SCE reference electrode. The F_c^+/F_c potential ($E_{1/2} = (E_{p,a} + E_{p,c})/2$) was 0.52 V in CH_2Cl_2 at the glassy-carbon electrode (ΔE_p = 160 mV; 100 mV s^{-1}) and at the Pt electrode (ΔE_p = 235 mV; 100 mV s^{-1}). Differential-pulse polarography was carried out under the following conditions: modulation amplitude 10 mV, one pulse/s, scan rate 5 mV/s. Purified nitrogen was used to purge the solutions prior to electrochemical measurements. Proton NMR spectra were recorded on a Bruker WH-300 Fourier transform instrument. Visible–UV spectra were obtained on a Varian Cary 17 and/or a Perkin-Elmer 551S spectrophotometer. The magnetic susceptibilities of powdered samples were determined at three different temperatures (293, 195, and 90 K) and different magnetic fields (1.26, 2.59, 3.78, and 5.06 kG) by the standard Gouy technique.[20] The susceptibility data were corrected for molecular diamagnetism by use of Pascal's constants.[21] The values for the correction of the metal ions were taken from ref 20.

Results and Discussion

Synthesis. The reaction of the divalent metal ions Fe^{2+} and Mn^{2+} with a 2-fold excess of the sodium salt of toluene-3,4-dithiol in methanol yields monomeric, extremely air-sensitive $[M(tdt)_2]^{2-}$ complexes, which can be isolated as Ph_4P^+ salt in good yields. Hitherto the existence of the monomeric $[Fe(tdt)_2]^{2-}$ anion has been demonstrated only in solution. It was first detected by polarography in dichloromethane[26] and later prepared by electrochemical reduction[3] but was never isolated from the reaction solution. The nonmethylated derivative $[Fe(bdt)_2]^{2-}$ was recently prepared by reaction of $Li_2S_2C_6H_4$ and $FeCl_2$ in tetrahydrofuran.[27]

Controlled aerial oxidation of the $Na_2[M(tdt)_2]$ complexes dissolved in methanol affords the dimeric $[Fe_2(tdt)_4]^{2-}$ anion in the iron system and both of the mononuclear M(III) complexes $[Mn(tdt)_2]^-$ and $[Mn(tdt)_2MeOH]^-$ in the manganese system. All these complexes were separated from the reaction solution by addition of Ph_4PBr. A more convenient synthesis has been described earlier for $[Fe_2(tdt)_4]^{2-}$[28a–c] and more recently for $[Fe_2(bdt)_4]^{2-}$,[28d] using $FeCl_3$ as starting material. This preparation, taking advantage of iron in a higher oxidation state, avoids the additional oxidation step and therefore the formation of higher oxidized byproducts. Unfortunately, a comparably suitable M(III) precursor was not found for the Mn/tdt^{2-} system. The use of air oxygen in the preparation of the $Mn(III)/tdt^{2-}$ complexes afforded an intractable and insoluble byproduct, which could easily be removed by filtration.

(22) (a) Sparks, R. In *Computational Needs and Resources in Crystallography*; National Academy of Sciences: Washington, DC, 1973; pp 66–75. (b) SHELXTL program package, NICOLET XRD Corp., Madison, WI. (c) *International Tables for X-Ray Crystallography*; Kynoch Press: Birmingham, England, 1974; Vol. IV.
(23) Germain, G.; Main, P.; Woolfson, M. M. *Acta. Crystallogr., Sect. A: Cryst. Phys., Diffr., Gen. Theor. Crystallogr.* **1971**, *A27*, 368.
(24) Bustos, L.; Khan, M. A.; Tuck, D. G. *Can. J. Chem.* **1983**, *61*, 1146.
(25) Henkel, G.; Schmidt, W.; Krebs, B. Unpublished results.
(26) Balch, A. L.; Dance, I. G.; Holm, R. H. *J. Am. Chem. Soc.* **1968**, *90*, 1139.
(27) Sellmann, D.; Kleine-Kleffmann, U.; Zapf, L. *J. Organomet. Chem.* **1984**, *263*, 321.
(28) (a) Williams, R.; Billig, E.; Waters, J. H.; Gray, H. B. *J. Am. Chem. Soc.* **1966**, *88*, 43. The $[Fe_2(tdt)_4]^{2-}$ anion has been structurally characterized: (b) Henkel, G.; Tremel, W.; Kuhlmann, U.; Krebs, B. *Proc. Int. Conf. Coord. Chem.* **1980**, *21*, 351. (c) See ref 3. (d) Kang, B. S.; Weng, L. H.; Wu, D. X.; Wang, F.; Guo, Z.; Huang, L. R.; Huang, Z. Y.; Liu, H. Q. *Inorg. Chem.* **1988**, *27*, 1129.

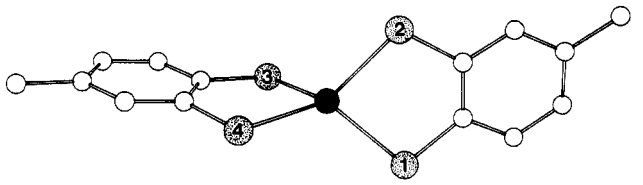

Figure 1. $[Ph_4P]_2[Mn(tdt)_2]\cdot 2MeOH$: Structure of the $[Mn(tdt)_2]^{2-}$ anion without H atoms.

Changing the ratio $MnCl_2$:tdt^{2-} gradually from 1:1 to 1:3 did not result in the formation of new products. We were unsuccessful in finding any evidence for the existence of the claimed $[Mn(tdt)_3]^{2-}$ complex[12] in the Mn/tdt^{2-} system upon aerial oxidation. In all cases the only product that could be isolated was **2**.

Description and Discussion of the Structures. The crystal structures of the two thiolate salts **1** and **2** (see Table I) consist of separated cations and anions. In both cases, noncoordinated methanol molecules are also present. The structures of the cations are unexceptional and will not be discussed here. For the purpose of clarity, the atoms in the two-dimensional representations of the anions are shown as spheres with arbitrary radii (Mn, black; S, dotted; C, white).

$[Mn(tdt)_2]^{2-}$. The structure of the $[Mn(tdt)_2]^{2-}$ anion is shown in Figure 1. The complex features an extremely distorted tetrahedral MnS_4 coordination unit with a dihedral angle of 89.07° between the two tdt^{2-} planes. Due to the short intraligand S···S distances of 3.384 Å (mean value) the S–Mn–S angles can be divided into two sets; set 1 contains the two chelate angles being close to 90° (mean value 88.87) and set 2 contains the four mixed-ligand ones being close to 120° (mean value 120.55). The mean Mn–S bond length of 2.417 Å in $[Mn(tdt)_2]^{2-}$ is 0.015 Å shorter than that in the $[Mn(edt)_2]^{2-}$ complex,[8] whose overall geometry nevertheless closely approaches that of $[Mn(tdt)_2]^{2-}$. The same type of coordination is also found for the d^{10} ions Cd^{2+}[24] and Hg^{2+}.[25]

$[Mn(tdt)_2]^-$ and $[Mn(tdt)_2MeOH]^-$. A stereoscopic view of the unit cell of **2** is given in Figure 2. Initially the composition of compound **2** led to the formulation as $[Ph_4P][Mn(tdt)_2]\cdot 2MeOH$. However, not one single type of anion, as implied by this formulation, is present but two different ones: $[Mn(tdt)_2]^-$ and $[Mn(tdt)_2MeOH]^-$. Their structures are depicted in Figure 3 with the corresponding atomic labeling schemes. Besides the anions there are two Ph_4P^+ cations and three methanol molecules in the asymmetric unit of the unit cell. As the hydroxylic H atom of the coordinated methanol ligand could not be refined successfully, it was uncertain which formal oxidation states had to be assigned to the metal ions. A methoxido ligand would have to be counterbalanced by a manganese(IV) center, thus requiring a mixed-valence Mn(III,IV) salt. This problem was finally solved spectroscopically (vide infra). In Table V selected bond distances and valence angles within the anions are listed.

Table II. $[Ph_4P]_2[Mn(tdt)_2]\cdot 2MeOH$: Atomic Coordinates of the $[Mn(tdt)_2]^{2-}$ Anion

atom	*x*	*y*	*z*
Mn	0.25998 (4)	0.16155 (8)	0.75319 (4)
S(1)	0.14425 (7)	0.16863 (13)	0.70382 (7)
S(2)	0.25034 (7)	−0.02344 (13)	0.78992 (7)
S(3)	0.32012 (7)	0.18393 (13)	0.68248 (7)
S(4)	0.32276 (7)	0.30736 (13)	0.82206 (7)
C(1)	0.1261 (3)	0.0279 (5)	0.7092 (3)
C(2)	0.1691 (3)	−0.0517 (5)	0.7454 (3)
C(3)	0.1471 (3)	−0.1599 (5)	0.7489 (3)
C(4)	0.0841 (3)	−0.1903 (5)	0.7173 (3)
C(5)	0.0426 (3)	−0.1123 (5)	0.6800 (3)
C(6)	0.0623 (3)	−0.0058 (5)	0.6752 (3)
C(7)	0.0629 (3)	−0.3051 (6)	0.7276 (3)
C(8)	0.3815 (3)	0.2718 (5)	0.7296 (3)
C(9)	0.3840 (3)	0.3241 (5)	0.7874 (3)
C(10)	0.4360 (3)	0.3897 (5)	0.8218 (3)
C(11)	0.4860 (3)	0.4094 (5)	0.7993 (3)
C(12)	0.4835 (3)	0.3576 (5)	0.7420 (3)
C(13)	0.4329 (3)	0.2921 (5)	0.7078 (3)
C(14)	0.5398 (3)	0.4856 (5)	0.8354 (3)

Table III. $[Ph_4P]_2[Mn(tdt)_2]\cdot 2MeOH$: Selected Distances and Angles of the $[Mn(tdt)_2]^{2-}$ Anion

	Distances (Å)		
	Mn–S		
Mn–S(1)	2.434 (2)	Mn–S(4)	2.425 (2)
Mn–S(2)	2.414 (2)	mean	2.417
Mn–S(3)	2.395 (2)		
	S···S		
S(1)···S(2)	3.385 (2)	mean	3.384
S(3)···S(4)	3.383 (2)		
	Angles (deg)		
	S–Mn–S		
S(1)–Mn–S(3)	117.41 (7)	S(1)–Mn–S(2)	88.59 (6)
S(1)–Mn–S(4)	123.06 (7)	S(3)–Mn–S(4)	89.15 (6)
S(2)–Mn–S(3)	117.13 (7)	mean	88.87
S(2)–Mn–S(4)	124.59 (7)	mean of all	109.98
mean	120.55		

The $[Mn(tdt)_2]^-$ anion is almost exactly planar if the hydrogen atoms of the methyl groups are neglected; the largest atom displacement from the unweighted least-squares plane throughout

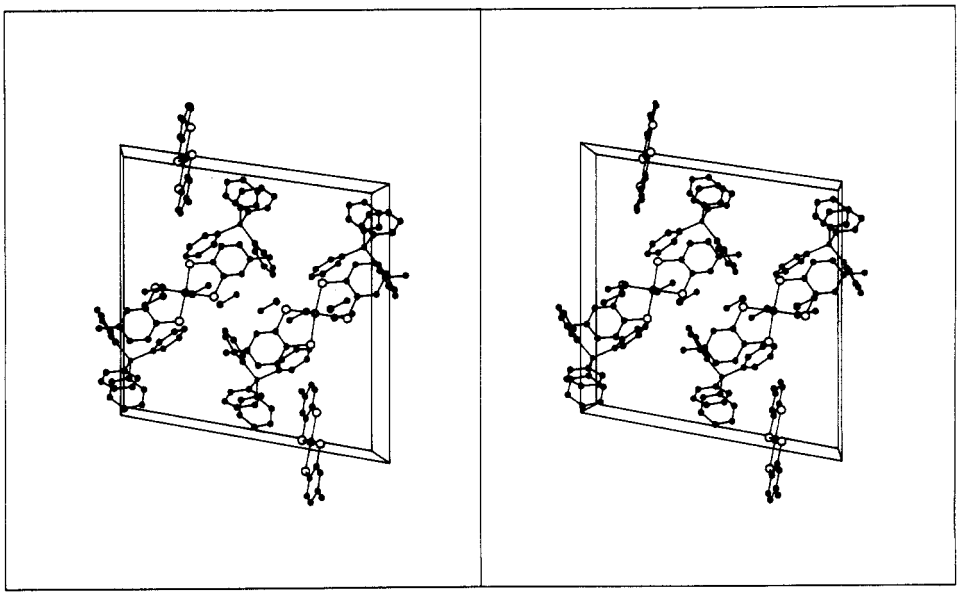

Figure 2. $[Ph_4P]_2[Mn(tdt)_2][Mn(tdt)_2MeOH]\cdot 3MeOH$: A stereoscopic view of the unit cell.

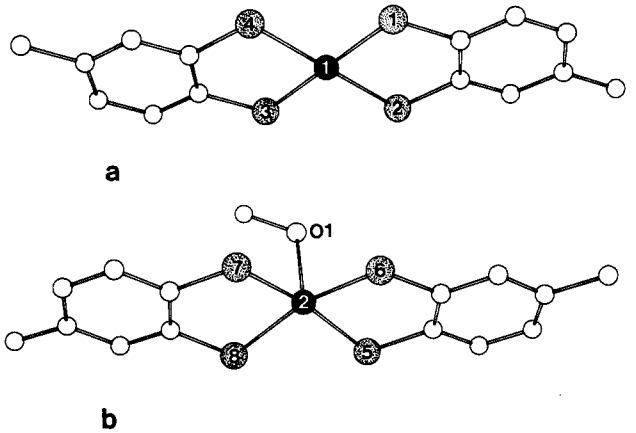

Figure 3. $[Ph_4P]_2[Mn(tdt)_2][Mn(tdt)_2MeOH]\cdot 3MeOH$: Structures of the anions $[Mn(tdt)_2]^-$ (a) and $[Mn(tdt)_2MeOH]^-$ (b) without H atoms.

Table IV. $[Ph_4P]_2[Mn(tdt)_2][Mn(tdt)_2MeOH]\cdot 3MeOH$: Atomic Coordinates of the $[Mn(tdt)_2]^-$ and $[Mn(tdt)_2MeOH]^-$ Anions

atom	x	y	z
		$[Mn(tdt)_2]^-$	
Mn(1)	0.24917 (5)	0.25012 (3)	−0.00154 (2)
S(1)	0.27237 (7)	0.27321 (4)	0.11512 (4)
S(2)	0.45959 (8)	0.22380 (4)	−0.00775 (4)
S(3)	0.22551 (7)	0.22669 (4)	−0.11828 (4)
S(4)	0.03889 (8)	0.27637 (4)	0.00465 (4)
C(1)	0.4401 (3)	0.2636 (1)	0.1318 (1)
C(1A)	0.0576 (3)	0.2361 (1)	−0.1346 (1)
C(2)	0.5211 (3)	0.2414 (1)	0.0787 (1)
C(2A)	−0.0231 (3)	0.2582 (1)	−0.0816 (1)
C(3)	0.6513 (3)	0.2331 (1)	0.0942 (1)
C(3A)	−0.1541 (3)	0.2660 (2)	−0.0973 (2)
C(4)	0.7034 (3)	0.2457 (2)	0.1616 (2)
C(4A)	−0.2076 (3)	0.2526 (2)	−0.1640 (2)
C(5)	0.6219 (3)	0.2680 (2)	0.2137 (1)
C(5A)	−0.1254 (3)	0.2309 (2)	−0.2165 (1)
C(6)	0.4932 (3)	0.2772 (2)	0.1990 (1)
C(6A)	0.0047 (3)	0.2225 (2)	−0.2022 (1)
C(7)	0.8441 (3)	0.2359 (2)	0.1770 (2)
C(7A)	−0.3490 (3)	0.2610 (2)	−0.1796 (2)
		$[Mn(tdt)_2MeOH]^-$	
Mn(2)	0.27193 (5)	0.74571 (3)	0.49891 (2)
S(5)	0.24330 (8)	0.77073 (4)	0.61556 (4)
S(6)	0.33782 (12)	0.86807 (5)	0.49970 (4)
S(7)	0.24828 (8)	0.72756 (4)	0.38103 (4)
S(8)	0.13544 (8)	0.63061 (4)	0.49613 (4)
O(1)	0.4769 (2)	0.7205 (1)	0.5019 (1)
C(O1)	0.4980 (3)	0.6572 (2)	0.4578 (2)
C(8)	0.3173 (3)	0.8640 (2)	0.6382 (2)
C(8A)	0.1781 (3)	0.6336 (2)	0.3590 (2)
C(9)	0.3596 (3)	0.9063 (2)	0.5878 (2)
C(9A)	0.1287 (3)	0.5914 (2)	0.4086 (2)
C(10)	0.4159 (4)	0.9809 (2)	0.6069 (2)
C(10A)	0.0741 (3)	0.5175 (2)	0.3886 (2)
C(11)	0.4280 (3)	0.0135 (2)	0.6756 (2)
C(11A)	0.0684 (3)	0.4839 (2)	0.3208 (2)
C(12)	0.3869 (3)	0.9709 (2)	0.7250 (2)
C(12A)	0.1160 (3)	0.5261 (2)	0.2715 (2)
C(13)	0.3325 (3)	0.8973 (2)	0.7071 (2)
C(13A)	0.1702 (3)	0.6000 (2)	0.2901 (2)
C(14)	0.4845 (4)	0.0941 (2)	0.6956 (2)
C(14A)	0.0148 (3)	0.4030 (2)	0.3004 (2)

the whole anion is less than 0.08 Å. Besides a small dihedral angle of 0.67° between the two tdt^{2-} ligands, idealized $\bar{1}$ symmetry is nearly achieved. The two methyl groups also follow this symmetry. The four Mn–S bonds, which average to 2.282 Å, are virtually identical.

The two sets of S–Mn–S angles, the first one involving angles of adjacent S atoms and the second one angles between S atoms in the trans position, have mean values of 90.00 and 179.93°, respectively. As even the mean interligand S···S distance of 3.220 Å is only slightly shorter (by 0.012 Å) than the mean intraligand

Table V. $[Ph_4P]_2[Mn(tdt)_2][Mn(tdt)_2MeOH]\cdot 3MeOH$: Selected Distances and Angles in the $[Mn(tdt)_2]^-$ and $[Mn(tdt)_2MeOH]^-$ Anions

		Distances (Å)	
		$[Mn(tdt)_2]^-$ Anion	
		Mn–S	
Mn(1)–S(1)	2.280 (1)	Mn(1)–S(4)	2.281 (1)
Mn(1)–S(2)	2.283 (1)	mean	2.282
Mn(1)–S(3)	2.282 (1)		
		S···S	
S(1)···S(2)	3.233 (1)	S(1)···S(4)	3.219 (1)
S(3)···S(4)	3.231 (1)	S(2)···S(3)	3.221 (1)
mean	3.232	mean	3.220
		$[Mn(tdt)_2MeOH]^-$ Anion	
		Mn–S	
Mn(2)–S(5)	2.314 (1)	Mn(2)–S(8)	2.312 (1)
Mn(2)–S(6)	2.306 (1)	mean	2.309
Mn(2)–S(7)	2.306 (1)		
		Mn–O	
Mn(2)–O(1)	2.224 (2)		
		S···S	
S(5)···S(6)	3.214 (1)	S(5)···S(8)	3.255 (1)
S(7)···S(8)	3.230 (1)	S(6)···S(7)	3.233 (1)
mean	3.222	mean	3.244
		Angles (deg)	
		$[Mn(tdt)_2]^-$ Anion	
		S–Mn–S	
S(1)–Mn(1)–S(2)	90.23 (3)	S(1)–Mn(1)–S(3)	179.86 (4)
S(1)–Mn(1)–S(4)	89.77 (3)	S(2)–Mn(1)–S(4)	180.00 (4)
S(2)–Mn(1)–S(3)	89.81 (3)	mean	179.93
S(3)–Mn(1)–S(4)	90.18 (3)		
mean	90.00		
		$[Mn(tdt)_2MeOH]^-$ Anion	
		S–Mn–S	
S(5)–Mn(2)–S(6)	88.16 (4)	S(5)–Mn(2)–S(7)	165.78 (4)
S(5)–Mn(2)–S(8)	89.45 (3)	S(6)–Mn(2)–S(8)	161.17 (4)
S(6)–Mn(2)–S(7)	88.99 (4)	mean	163.48
S(7)–Mn(2)–S(8)	88.76 (3)		
mean	88.84		
		S–Mn–O	
S(5)–Mn(2)–O(1)	98.74 (6)	S(8)–Mn(2)–O(1)	98.17 (6)
S(6)–Mn(2)–O(1)	100.65 (6)	mean	98.26
S(7)–Mn(2)–O(1)	95.48 (6)		

one, the coordination geometry is adequately described as square-planar.

The addition of a methanol molecule to the planar $\{Mn(tdt)_2\}$ moiety extends the coordination sphere of manganese to a square pyramid, whose apex is occupied by the O atom, while the S atoms define the basal plane. Structural features of the resulting $[Mn(tdt)_2MeOH]^-$ anion can be summarized with respect to $[Mn(tdt)_2]^-$ as follows. (i) Mn–S distances are slightly longer (2.309 vs 2.282 Å). (ii) The metal atom is shifted by 0.33 Å out of the basal plane toward the methanol ligand. (iii) The dihedral angle increases to about 4°. The mean value of the four Mn–S distances is only slightly shorter (by 0.009 Å) than the mean value of the three terminal Mn–S distances in the dimeric $[Mn_2(edt)_4]^{2-}$ complex in which the pentacoordination of Mn(III) is accomplished via short (2.346 Å) and long (2.632 Å) sulfur bridges. A shortening of metal–sulfur distances in tdt^{2-} complexes compared to their counterparts in complexes containing saturated edt^{2-} ligands is observed not only in the manganese(II,III) system but also for iron and vanadium.[16,17] This could reflect the better π-donor capacity of the aromatic dithiolate ligand, which allows electron delocalization within the whole $M_2S_2C_2$ chelate ring. However, as there are neither significant deviations from common mean values for C–S and C–C distances nor significant differences among the C–C distances in the ring system, it seems justified by crystallographic arguments to locate the oxidation mainly on the metal centers and not on the ligands. This interpretation, which is different from that given in ref 3, is further supported by the magnetic behavior (see below) and by the observation that

Table VI. Proton Resonance Signals and Their Assignment for the $[M(tdt)_2]^{n-}$ (M = Fe, Mn) and $[Mn(bdt)_2]^-$ Anions ($(CD_3)_2SO$ Solutions at 296 K)

	δ, ppm		
$[Mn(tdt)_2]^-$ and $[Mn(tdt)_2MeOH]^-$	−15.7 (CH_3)	4.6 (3-H) 9.3 (6-H)	20.8 (5-H)
$[Mn(bdt)_2]^-$		7.0 (3-H, 6-H)	21.8 (4-H, 5-H)
$[Fe(tdt)_2]^-$	−25.3 (CH_3)	34.1, 30.0 (3-H, 5-H, 6-H)	
$[Fe(tdt)_2]^{2-}$	−15.6 (CH_3)	−13.3 (3-H) −12.4 (6-H)	9.3 (5-H)

the Mn–S distances in both anions of **2** are not compatible with one unique Mn–S bond per complex anion.

Magnetic Properties. The solid-state magnetic moment of 6.15 μ_B for **1** reveals the typical high-spin behavior of monomeric manganese complexes with tetrahedral thiolate-sulfur coordination and d^5 configuration. Other examples are $[Et_4N]_2[Mn(edt)_2]$,[8] $[Et_4N]_2[Mn(SPh)_4]$,[7] and the mixed chloride–thiolate complex $[Et_4N]_2[MnCl(SPh)_3]$.[9]

In the solid state **2** exhibits Curie behavior with a magnetic moment (corrected for diamagnetism) of 5.2 μ_B (spin-only value of a d^4 system 4.9 μ_B). The same value has been reported recently for the $[Mn(tdt)_2]^-$ anion in Me_2SO solution.[3] There is no evidence for an increase in magnetic moment at higher temperature, as would be expected for an electronically coupled Mn(II)/semiquinone complex. The complex salt $Na[Mn(DTBC)_2]\cdot 4CH_3CN$ containing di-*tert*-butylcatecholate ($DTBC^{2-}$), an oxo analogue of the tdt^{2-} ligand, has a magnetic moment of 5.1 μ_B, which was assigned to a trivalent metal center.[29] The magnetic moments of manganese(III)/porphyrin or -/phthalocyanine complexes with a ligand-enforced square-planar metal coordination, which is sometimes expanded by axial ligands, are usually found in the range 4.7–5.3 μ_B.[30] By transition from Mn(III) to Mn(IV) the magnetic moments of these complexes drop considerably below 4.0 μ_B.[30] With respect to these data we interpret the magnetic susceptibility in terms of two manganese(III) centers in two different (crystallographically proven) coordination environments.

Proton NMR Spectra. The ^1H NMR spectra provide further characterization of **2** and elucidate the problem of assigning oxidation states to the metal ions (vide supra). Four distinct isotropically shifted signals are found for the protons of the $[Mn(tdt)_2]^-$ anion in CD_3CN and in $(CD_3)_2SO$. No (shifted) signal was found that could be assigned to a coordinated methanol or methanolate ligand. These observations are consistent with a rapid exchange of the neutral methanol ligand in $[Mn(tdt)_2MeOH]^-$ by solvent molecules. A representative spectrum of **2** in CD_3CN at 323 K is shown in Figure 4a.

Assignment of the resonances (Table VI) was established by comparison of the spectrum of **2** in $(CD_3)_2SO$ with the spectrum of $[Ph_4P][Mn(bdt)_2]$ in $(CD_3)_2SO$, which is depicted in Figure 4b. For the symmetric bdt^{2-} ligand the resonances for 3-H and 6-H, and for 4-H and 5-H, coincide high-field shifted at 7.0 and 21.8 ppm, respectively. For the 4-methylated tdt^{2-} ligand signals appear separately and poorly resolved at 4.6 and 9.3 ppm (3-H, 6-H), and at 20.8 ppm (5-H), with the methyl group giving rise to a sharp low-field signal at −15.7 ppm. The same shift pattern is also found for $[Ph_4P]_2[Fe_2(tdt)_4]$ for which a monomeric structure in Me_2SO has been established.[26,28]

The changing shift pattern for the methyl group in **2** and the corresponding proton in its bdt^{2-} derivative is indicative of π-delocalization of unpaired spin density and dominant contact interaction.[32] The temperature dependence of the shifts (Figure

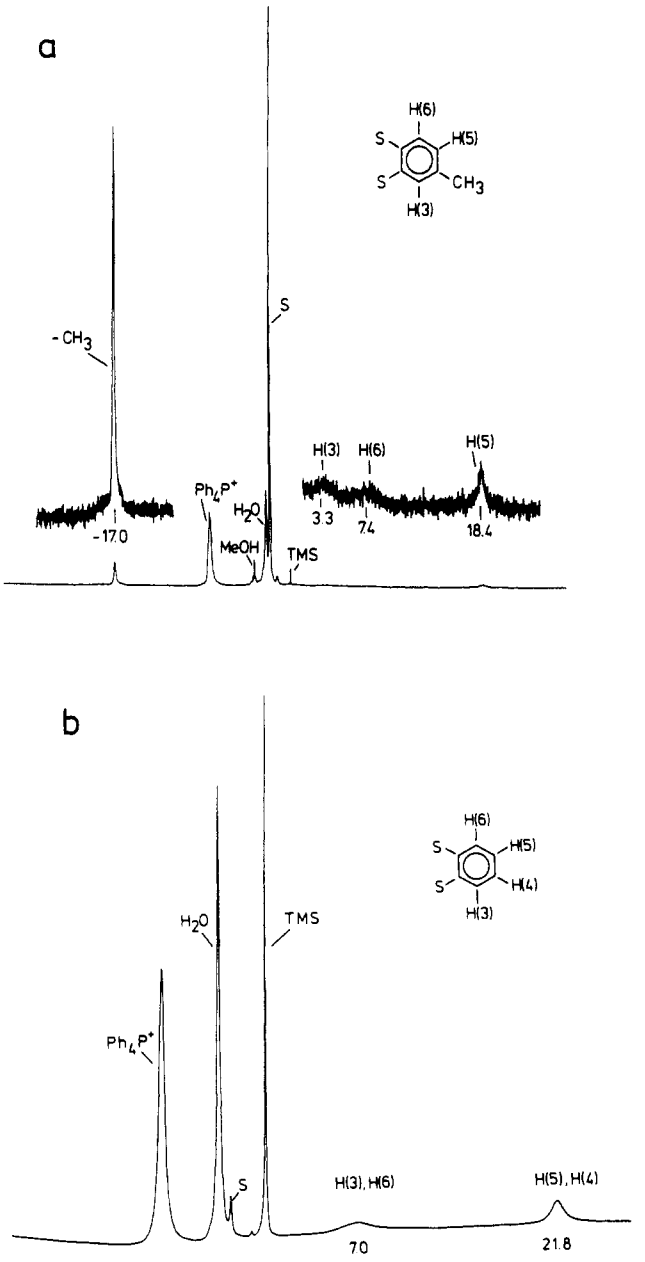

Figure 4. FT ^1H NMR spectra (300 MHz) of $[Mn(tdt)_2]^-$ in CD_3CN at 323 K (a) and of $[Mn(bdt)_2]^-$ in $(CD_3)_2SO$ at 296 K (b).

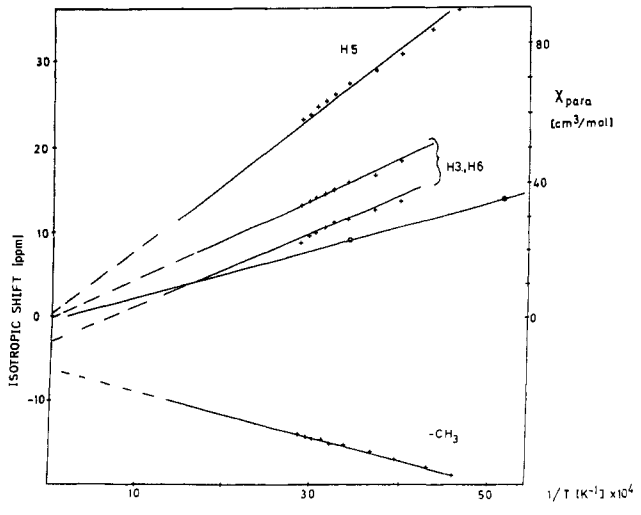

Figure 5. Temperature dependence of the proton isotropic shifts in CD_3CN (+) and of the solid-state magnetic susceptibility (○) of $[Ph_4P]_2[Mn(tdt)_2][Mn(tdt)_2MeOH]\cdot 3MeOH$.

(29) Chin, D.-H.; Sawyer, D. T.; Schaefer, W. P.; Simmons, C. J. *Inorg. Chem.* **1983**, *22*, 752.
(30) (a) Lever, A. B. P. *J. Chem. Soc., Dalton Trans.* **1965**, 1821. (b) Boucher, L. J. *Coord. Chem. Rev.* **1972**, *7*, 289. (c) Hatano, K.; Anzai, K.; Iitaka, Y. *Bull. Chem. Soc. Jpn.* **1983**, *56*, 422.
(31) Davis, T. S.; Fackler, J. P.; Weeks, M. J. *Inorg. Chem.* **1968**, *7*, 1994.
(32) Horrocks, W. D., Jr. In *NMR of Paramagnetic Molecules*; LaMar, G. N., Horrocks, W. D., Holm, R. H., Eds.; Academic Press: New York, 1973; Chapter 4.

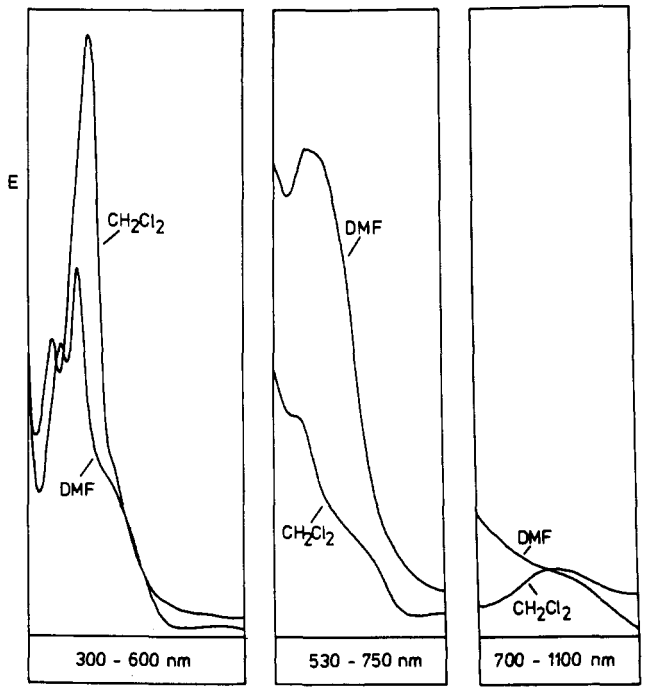

Figure 6. UV–visible absorption spectra of $[Ph_4P]_2[Mn(tdt)_2][Mn(tdt)_2MeOH]\cdot 3MeOH$ in *N,N*-dimethylformamide (DMF) and in CH_2Cl_2.

Table VII. $[Ph_4P]_2[Mn(tdt)_2][Mn(tdt)_2MeOH]\cdot 3MeOH$: UV–Vis Absorption Data for *N,N*-Dimethylformamide (DMF) and CH_2Cl_2 Solutions

DMF		CH_2Cl_2	
λ_{max}, nm	ϵ_M, M^{-1} cm^{-1}	λ_{max}, nm	ϵ_M, M^{-1} cm^{-1}
900 (sh)	200	900	215
570 (sh)	2200	640 (sh)	390
560	2300	540 (sh)	990
400 (sh)	7400	410 (sh)	12000
351	16300	370	40800
327	12600	315	19800

5) follows the Curie law with different zero intercepts. The increase in shifts at lower temperature is characteristic of a paramagnetic center. As the magnetic results (vide supra) clearly point out that only one spin state is populated ($S = 2$), a temperature-dependent coupling constant, as seen for $[Co(bdt)_2]^-$,[33] has to be taken into account.

Within the chelated dithiolate structure, spin can be polarized through both sulfur atoms. The aromatic protons of the tdt^{2-} ligand, however, are related differently to each sulfur atom. All protons have a meta position with respect to one sulfur atom and either an ortho or a para position with respect to the other one. The two spin polarization pathways operative are best illustrated by comparing the spectra of $[Fe(tdt)_2]^{2-}$ and $[Mn(tdt)_2]^-$ (Table VI): H-3 and H-6 are shifted to higher fields for the manganese compound, reflecting the dominance of the ortho position, while in the iron compound the meta position is determining the sign of the shifts. The signals are downfield shifted to −13.3 and −12.4 ppm. No spectrum could be recorded for $[Ph_4P]_2[Mn(tdt)_2]\cdot 2MeOH$.

Electronic Spectra. UV–vis spectra of **2** in *N,N*-dimethylformamide (DMF) and CH_2Cl_2 are presented in Figure 6 and summarized in Table VII. The spectra are remarkably solvent-dependent with respect to the band positions, intensities, and shapes, but the principal absorption pattern remains essentially the same. These observations conform to different species in solution. The strongly coordinating solvent DMF not only can replace the methanol molecule in $[Mn(tdt)_2MeOH]^-$ but also may extend the ligand environment of the metal atoms in **2** to an octahedral coordination. In the noncoordinating solvent CH_2Cl_2 even the formation of dimers, as established for $Fe(III)/tdt^{2-}$,[26] is conceivable. The broad low-intensity absorptions at 900 nm are typical for Mn(III) compounds and due to d–d transitions.[31] The bands between 500 and 700 nm originate probably (mainly) in charge-transfer processes, while the bands at higher energy are presumably due to intraligand transitions.

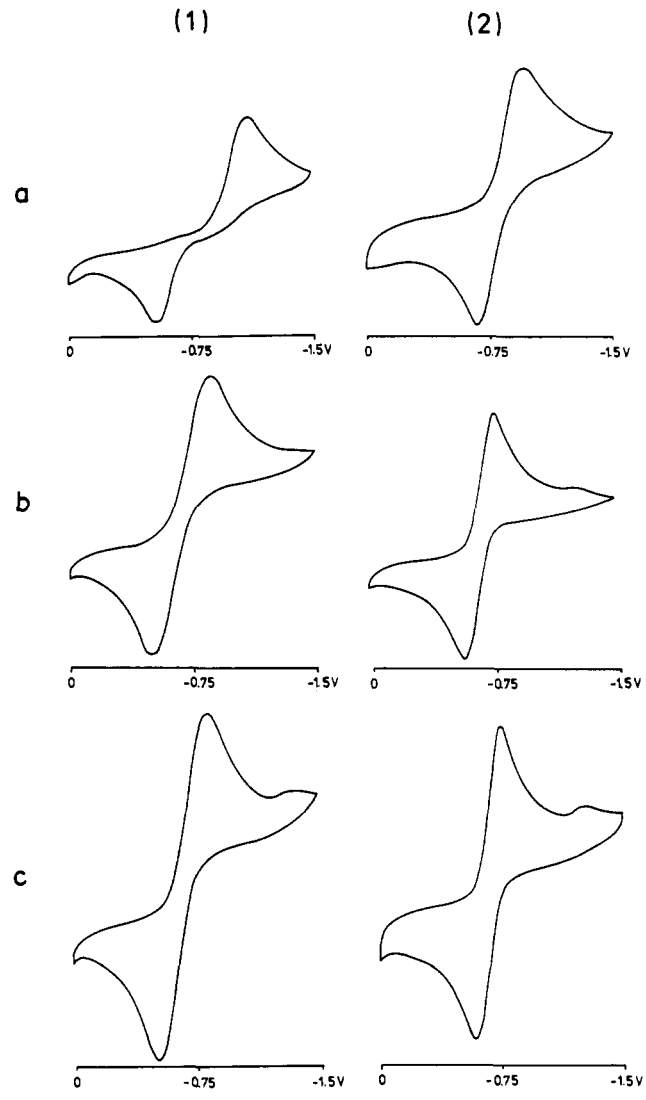

Figure 7. Cyclic voltammograms of $[Ph_4P]_2[Mn(tdt)_2][Mn(tdt)_2MeOH]\cdot 3MeOH$ in DMF (a), CH_2Cl_2 (b), and $C_2H_4Cl_2$ (c) at the Pt-flag (1) and the glassy-carbon (2) electrodes.

Table VIII. $[Ph_4P]_2[Mn(tdt)_2][Mn(tdt)_2MeOH]\cdot 3MeOH$: Peak Maxima (V vs Saturated Calomel Electrode) in the Cyclic Voltammograms

process	solvent		
	$C_2H_4Cl_2$	CH_2Cl_2	DMF
Pt Electrode, 0.1 M Bu_4NClO_4, Scan Speed 100 mV/s			
redn ($E_{p,c}$)	−0.85	−0.88	−1.10
oxidn ($E_{p,a}$)	−0.51	−0.50	−0.53
Glassy-Carbon Electrode, 0.1 M Bu_4NClO_4, Scan Speed 100 mV/s			
redn ($E_{p,c}$)	−0.75	−0.78	−0.96
oxidn ($E_{p,a}$)	−0.58	−0.58	−0.67

Electrochemistry. Figure 7 illustrates the quite remarkably solvent- and electrode-dependent Mn(II)/Mn(III) redox couple in the cyclic voltammograms of **2**. In all cases current is conserved over the potential range as indicated by the $i_{p,c}$:$i_{p,a}$ ratio, which comes very close to unity. Electrochemical properties are summarized in Table VIII.[36,37]

(33) Put, P. J.; Schilperoord, A. A. *Inorg. Chem.* **1974**, *13*, 2476.
(34) Parry, E. P.; Osteryoung, R. A. *Anal. Chem.* **1965**, *37*, 1634.
(35) Mukherjee, R. N.; Pulla Rao, C.; Holm, R. H. *Inorg. Chem.* **1986**, *25*, 2979.

The redox properties of the Mn(II)/Mn(III) transition were further investigated by polarography in CH_2Cl_2. Plots of log $[i/(i_d - i)]$ vs E for the first reduction yield slopes that are acceptably close to the theoretical value of 59 mV for a one-electron transfer at 25 °C. This result was confirmed by differential-pulse polarography measurements in CH_2Cl_2 and $C_2H_4Cl_2$.[37] The half-widths of 88 and 110 mV in CH_2Cl_2 and $C_2H_4Cl_2$, respectively, leave little doubt about the presence of a one-electron process (for which a theoretical value of 90.4 mV is expected) rather than a two-electron step.[34] This behavior is consistent with a one-electron oxidation of the $[Mn(tdt)_2]^{2-}$ complex to a Mn(III) species, but all electrochemical data for **2** provide no evidence for the existence of any stable Mn(IV) species. Any tentative assignment of different oxidation states to the metal ions of the two chemically different complexes present in **2** can therefore be excluded.

The Pt electrode provides in all solvents much larger peak separations in the cyclic voltammograms of **2** than the glassy-carbon electrode. The same electrode effect on ΔE_p values was observed for the $[Mn_2(edt)_4]^{2-}$ ($[Mn(edt)_2(Me_2SO)_2]$)/$[Mn(edt)_2]^{2-}$ redox couple and assigned to a much smaller rate constant for the heterogeneous electron transfer at the Pt electrode.[35] Within the group of related M(II,III)/edt^{2-} and M(II,III)/tdt^{2-} complexes (M = Co, Fe, Mn), the manganese compounds exhibit the most pronounced electrode dependences in their CV characteristics. In addition, the ΔE_p values and redox potentials are strongly affected by the solvent. In CH_2Cl_2 (and in $C_2H_4Cl_2$) much smaller ΔE_p and less negative $E_{1/2}$ values are found than in DMF under similar conditions. The stronger interactions of better coordinating solvents (e.g. DMF vs CH_2Cl_2) with the planar $[Mn(tdt)_2]^-$ anions of **2** result in redox potentials that are more negative. The same arguments can be used to explain the smaller peak separation and the less cathodic potential for the Mn(II)/Mn(III) redox couple in DMF compared to Me_2SO.[35]

Acknowledgment. This work was supported by the Minister für Wissenschaft und Forschung des Landes Nordrhein-Westfalen, the Bundesminister für Forschung und Technologie (BMFT) under Contract No. 05339 GAB/3, and the Fonds der Chemischen Industrie. We are grateful to Dr. H. Strasdeit for valuable comments and discussions.

Supplementary Material Available: Positional and thermal parameters of the anions, cations, and solvate molecules (Tables S-I and S-IV), complete distances and angles within the anions, cations, and solvate molecules (Tables S-II and S-V), and details of data collection and structure refinements (Table S-VII) (19 pages); observed and calculated structure factors (Tables S-III and S-VI) (86 pages). Ordering information is given on any current masthead page.

(36) With the Pt-flag electrode another solvent-dependent reduction is seen at a very low potential (DMF, −1.80 V; CH_2Cl_2, −1.55 V) without any corresponding oxidation wave. In addition, a single oxidation wave at higher potential occurs (DMF, 0.33 V; CH_2Cl_2, 0.35 V).

(37) To exclude the possibility that CH_2Cl_2 may serve as a chloride donor for redox-active **2**, cyclic voltammograms and polarograms of **2** in 1,2-dichloroethane ($C_2H_4Cl_2$) and dichloromethane (CH_2Cl_2) were recorded. No substantial solvent-dependent differences, however, could be detected.

Contribution from the Departments of Chemistry, Thimann Laboratories, University of California, Santa Cruz, California 95064, and University of California, Davis, California 95616

Novel Chiral Trinuclear and Symmetric Tetranuclear Imidazolate-Bridged Cobalt(III) Complexes of a Synthetic Analogue of Bleomycin

Steven J. Brown, Marilyn M. Olmstead,† and Pradip K. Mascharak*

Received January 17, 1989

Attempts to synthesize the cobalt(III) complex of PMAH (**2**), a designed ligand that mimics a major portion of the metal-chelating locus of the antitumor drug Bleomycin (BLM, **1**), have afforded two novel imidazolate-bridged trimeric and tetrameric complexes. The trimeric complex $[Co(L)]_3Cl(BF_4)_2 \cdot 9.25H_2O$ (**3**) (L = $PMAH_{-2H}$) crystallizes in the space group $R3$ with a = 40.838 (11) Å, c = 12.975 (3) Å, V = 18741 (8) Å^3, and Z = 12. The cation in **3** has 3-fold symmetry and is chiral. The chloride ion, which sits on the 3-fold axis, forms an intimate ion pair with the cation through hydrogen bonding. The tetrameric complex $[Co(L)]_4(BF_4)_4 \cdot 10DMF$ (**4**) crystallizes in the space group $P4/n$ with a = 21.436 (3) Å, c = 12.601 (3) Å, V = 5790 (2) Å^3, and Z = 2. In **4**, the cation has 4-fold symmetry and is optically inactive. The geometry at each cobalt(III) is approximately octahedral in both structures. Five nitrogen donor atoms from the doubly deprotonated ligand $PMAH_{-2}$ (L) occupy five coordination sites around each cobalt, while the sixth site is filled by the second nitrogen of the imidazole moiety of a neighboring unit. In aqueous and DMSO solutions, **3** exhibits strong CD signals. That both complex cations remain intact in solution has been checked by spectroscopic techniques including ^1H–^1H and ^1H–^{13}C COSY experiments. The structural and spectroscopic parameters of **3** and **4** are expected to provide help in elucidation of the structure(s) of Co^{III}–BLM.

Introduction

Bleomycins (BLM, **1**) are a family of glycopeptide antibiotics that are used in the treatment of certain types of cancer.[1] In the presence of a metal ion like Fe^{2+} and molecular oxygen, BLM inflicts single- and double-strand breaks in cellular DNA,[2-9] and the metal ion promoted DNA strand scission is assumed to be related to the drug action. Though the fact that metal chelates of BLM (metallobleomycins, M–BLMs) play a vital role in the complex drug–DNA chemistry is an accepted one, structural information on the architecture of the coordination spheres of the metal ions in M–BLMs remains rather elusive. Macromolecular M–BLMs have not been crystallized, and the coordination structures of M–BLMs have been predicted primarily on the basis of spectroscopic data.[2-9] In our "synthetic analogue approach"[10]

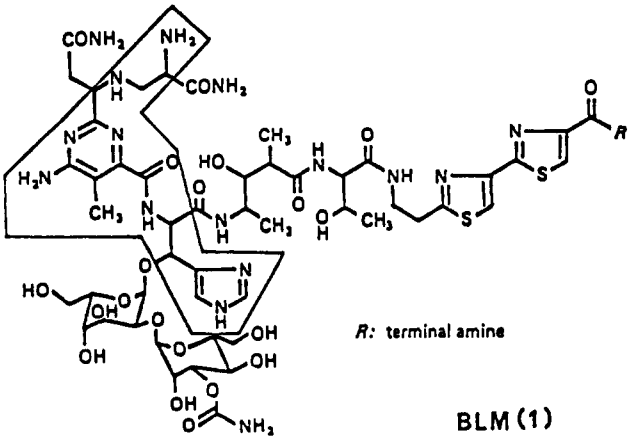

BLM (1)

to this problem, we are involved in determination of structures and reactivities of smaller model compounds (or analogues) that

* To whom correspondence should be addressed at the University of California, Santa Cruz.
† University of California, Davis.

0020-1669/89/1328-3720$01.50/0